Structure
Article

Allosteric Regulation of DNA Cleavage and Sequence-Specificity through Run-On Oligomerization

Dmitry Lyumkis,[1] Heather Talley,[2] Andrew Stewart,[2,3] Santosh Shah,[2] Chad K. Park,[2] Florence Tama,[2,4] Clinton S. Potter,[1] Bridget Carragher,[1,*] and Nancy C. Horton[2,*]
[1]National Resource for Automated Molecular Microscopy, Department of Integrative Structural and Computational Biology, The Scripps Research Institute, La Jolla, CA 92037, USA
[2]Department of Chemistry and Biochemistry
[3]Genetics Interdisciplinary Graduate Program
University of Arizona, Tucson, AZ 85721, USA
[4]Present address: RIKEN, Advanced Institute for Computational Sciences 7-1-26, Minatojima-minami-machi, Chuo-ku, Kobe, Hyogo 650-0047, Japan
*Correspondence: bcarr@scripps.edu (B.C.), nhorton@u.arizona.edu (N.C.H.)
http://dx.doi.org/10.1016/j.str.2013.08.012

SUMMARY

SgrAI is a sequence specific DNA endonuclease that functions through an unusual enzymatic mechanism that is allosterically activated 200- to 500-fold by effector DNA, with a concomitant expansion of its DNA sequence specificity. Using single-particle transmission electron microscopy to reconstruct distinct populations of SgrAI oligomers, we show that in the presence of allosteric, activating DNA, the enzyme forms regular, repeating helical structures characterized by the addition of DNA-binding dimeric SgrAI subunits in a run-on manner. We also present the structure of oligomeric SgrAI at 8.6 Å resolution, demonstrating the conformational state of SgrAI in its activated form. Activated and oligomeric SgrAI displays key protein-protein interactions near the helix axis between its N termini, as well as allosteric protein-DNA interactions that are required for enzymatic activation. The hybrid approach reveals an unusual mechanism of enzyme activation that explains SgrAI's oligomerization and allosteric behavior.

INTRODUCTION

The coevolution between parasitic phage and host bacterium represents one of nature's most extensive struggles for survival. Competitive environmental interactions have led both parasite and host to pursue intricate and diverse strategies of adaptation and counter-adaptation in what has been metaphorically described as an evolutionary arms race (Stern and Sorek, 2011). Like higher eukaryotes, host bacteria possess an innate, nonspecific immune system that accounts for the first line of defense against invading phage, which has given rise to numerous clever enzymatic mechanisms for selectively targeting and cleaving phage DNA. Restriction endonucleases (REases) are the enzymes that play a primary role in this mechanism for defense and are believed to have evolved specifically for this purpose (Pingoud and Jeltsch, 1997, 2001; Pingoud et al., 2005).

REases recognize and cleave duplex DNA and can be categorized into one of four different types (Roberts et al., 2010). The classical type II REase is homodimeric and cleaves DNA in a Mg^{2+}-dependent fashion at or near its 4–6 base-pair (bp) recognition sequence (Pingoud and Jeltsch, 1997, 2001; Pingoud et al., 2005). Of the ~4,000 categorized type II REases to date, only a small fraction cleave sequences containing more than 6 bp (Roberts et al., 2010). Due to the relative rarity of such cleavage sites, these enzymes have received particular attention, both for their interesting evolutionary properties (Bilcock et al., 1999) and for their value as tools for the analysis of genomic DNA (Qiang and Schildkraut, 1987). SgrAI is one such "rare-cutting" endonuclease, which recognizes three degenerate primary (or canonical) octanucleotide sequences that differ in the second and seventh bp—CGCCGGCG, CACCGGCG/CGCCGGTG, and CACCGGTG (Tautz et al., 1990). However, unlike any other REase, SgrAI will additionally cleave any of 17 secondary (or noncanonical) sequences [CPuCCGGPy(A/T/C) and CPuCCGGGG], but only in the presence of an activating primary site DNA containing a sufficient number of flanking bp (Bitinaite and Schildkraut, 2002; Park et al., 2010b; Wood et al., 2005). Thus, depending upon the input signal, the SgrAI REase can turn a rare DNA recognition sequence into one that is much more frequently encountered, dramatically increasing the number of DNA cleavages. How SgrAI can do this and the evolution of this mechanism is of considerable interest.

SgrAI maintains a baseline rate of cleavage for both primary and secondary sites, albeit one that is lower than its homologs (Bilcock et al., 1999; Park et al., 2010b). However, in the presence of multiple DNA cleavage sites, SgrAI acquires several properties that make the enzyme unique among known REases. First, it relaxes the requirement for highly defined nucleotide recognition sites, enabling the cleavage of a total of 17 degenerate DNA sequences through a process known as sequence-specificity expansion (Bitinaite and Schildkraut, 2002). Second, the rate of subsequent DNA cleavage for primary and secondary sites is accelerated by up to several orders of magnitude

(Hingorani-Varma and Bitinaite, 2003; Park et al., 2010b). Simultaneous sequence-specificity expansion and DNA cleavage rate acceleration have been more generally known as SgrAI activation (Park et al., 2010b). For activation to occur, DNA containing the primary cleavage site must be present (Bitinaite and Schildkraut, 2002). The DNA must also contain a minimum number of flanking bp (Park et al., 2010b; Wood et al., 2005). This indicates that substrate DNA itself plays the role of an allosteric effector within a positively cooperative and allosteric enzymatic reaction. Thus, previous studies have hypothesized that SgrAI must exhibit at least two conformational states to account for its self-activating behavior (Daniels et al., 2003; Dunten et al., 2008; Hingorani-Varma and Bitinaite, 2003; Park et al., 2010b). However, only the dimeric low activity form has been structurally characterized to date (Dunten et al., 2008; Little et al., 2011; Park et al., 2010a).

We present a structural, computational, and biochemical characterization of activated and oligomeric SgrAI. This hybrid approach provides insight into the enzyme's unusual manner of modulating activity through self-association into run-on oligomers—a phenomenon that is unique among REases. In addition, it reveals the high activity conformational state of the enzyme that suggests an evolutionary requirement for its mechanism of action within the context of innate prokaryotic immunity.

RESULTS

SgrAI Forms Run-On Oligomers in the Presence of Activating DNA

Previously, it has been shown that SgrAI activation can be achieved by the presence of activating DNA of any primary cleavage site containing a sufficient number of flanking bp. These include primary-site-containing plasmids (Bilcock et al., 1999; Bitinaite and Schildkraut, 2002; Wood et al., 2005), as well as uncleaved (Bitinaite and Schildkraut, 2002) and pre-cleaved (PC—containing sticky ends and resembling reaction products from DNA cleavage; Park et al., 2010b) synthetic DNA constructs. The activated species is heterogeneous and oligomeric in form, with an average size of ~700 kDa (Daniels et al., 2003; Park et al., 2010b). To investigate the structure of oligomeric SgrAI, we used transmission electron microscopy of negatively stained complexes of purified SgrAI and PC DNA that were prepared under conditions for promoting oligomerization (Park et al., 2010b). Individual particles observed in the images were highly heterogeneous in size (Figure S1 available online). Using an iterative workflow for aligning and reconstructing distinct populations of SgrAI oligomers (Lyumkis et al., 2013), we identified multiple classes of particles representing discrete oligomer lengths. The smallest particles were identified as an SgrAI DNA-binding dimer (DBD; Figure 1A), which forms the basic building block of the oligomer. Subsequently, two-dimensional (2D) class averages and corresponding three-dimensional (3D) reconstructions obtained using the random-conical tilt approach (Radermacher et al., 1986; 1987) were systematically arranged according to size, from a dimer of DBDs through a decamer of DBDs. Larger species, such as a tridecamer, become less well defined in the terminal regions due to flexibility along the particles (Figure 1B). The heterogeneous distribution of oligomers in the data favors smaller sizes, with particles containing more than ten DBDs becoming increasingly rare (Figure 1C). This analysis shows that the low activity SgrAI DBD that was previously characterized crystallographically (Dunten et al., 2008; Little et al., 2011; Park et al., 2010a) can oligomerize in a run-on fashion in the presence of activating DNA, supporting a current hypothesis from mass spectrometry data (Ma et al., 2013).

The Structure of Activated and Oligomeric SgrAI at 8.6 Å Resolution

Individual DBD subunits within each reconstructed oligomer are organized into a left-handed helix, with ~85 Å separation between adjacent subunits along the oligomeric Z axis. To improve the resolution of the electron microscopy (EM) density maps and to visualize DNA (which is not evident under most negative stain conditions; see Figures S3C and S3D), we prepared identical samples of SgrAI by vitrification and used cryo-EM to characterize the oligomers (Figure S2). Starting with the helical parameters measured from the 3D random-conical tilt reconstructions, we selected the largest helices identifiable within the cryo-micrographs and refined a data set of frozen hydrated oligomeric SgrAI to 8.6 Å resolution (Figures 2A and 2B; Figures S2 and S3; Movie S1). An SgrAI DBD makes up the basic helical asymmetric unit. The final helical parameters for the assembly were determined to be 21.6 Å rise and −86.2° twist, enabling slightly more than four DBD subunits to be built into a single turn of the helix (Figure 2A; Movie S1). At this resolution, the major and minor grooves of the B-form DNA, as well as most α-helical secondary structure elements of the protein are readily visible in the EM density maps (Figure 2C; Figure S2E). In conjunction with crystal structures of the low activity form of SgrAI (Dunten et al., 2008; Little et al., 2011; Park et al., 2010a), the structural details of the subnanometer resolution map enabled flexible fitting of the coordinates into the EM density (Figure 2D). The EM density can fully accommodate 12 of the 16 DNA flanking bp on either side of the helix. The outer bp likely becomes disordered, which can be seen by the gradual loss of density in the terminal regions (Figure 2D, arrows). Thus, the cryo-EM reconstruction together with flexible fitting provide approximate C-alpha coordinates for the activated and oligomeric form of SgrAI.

A Conformational Rearrangement Establishes Oligomer-Specific Interactions within Activated SgrAI

Previous analyses of activated SgrAI have focused on kinetic and biochemical properties of the enzyme, while its high-activity structure has remained elusive (Dunten et al., 2008; Little et al., 2011; Park et al., 2010a). Here, we present features of oligomeric SgrAI, characterized by single-particle electron microscopy and flexible fitting, which are specific to its high activity form.

Flexible fitting of the atomic coordinates of SgrAI (Dunten et al., 2008) into the 8.6 Å EM density map reveals notable rearrangement within several regions of the protein (Figure 3A). The overall root-mean-square deviation (rmsd) for the structure is 2.1 Å. To properly position the SgrAI backbone into the EM density, internal areas of the protein require little rearrangement (e.g., 1 Å rmsd for helix 247–268).However regions at, or in proximity to, critical protein-DNA interactions require greater rearrangement (e.g., 2.6 Å rmsd for loop 122–140; Table S1). Viewed from the outside of the oligomeric assembly, each

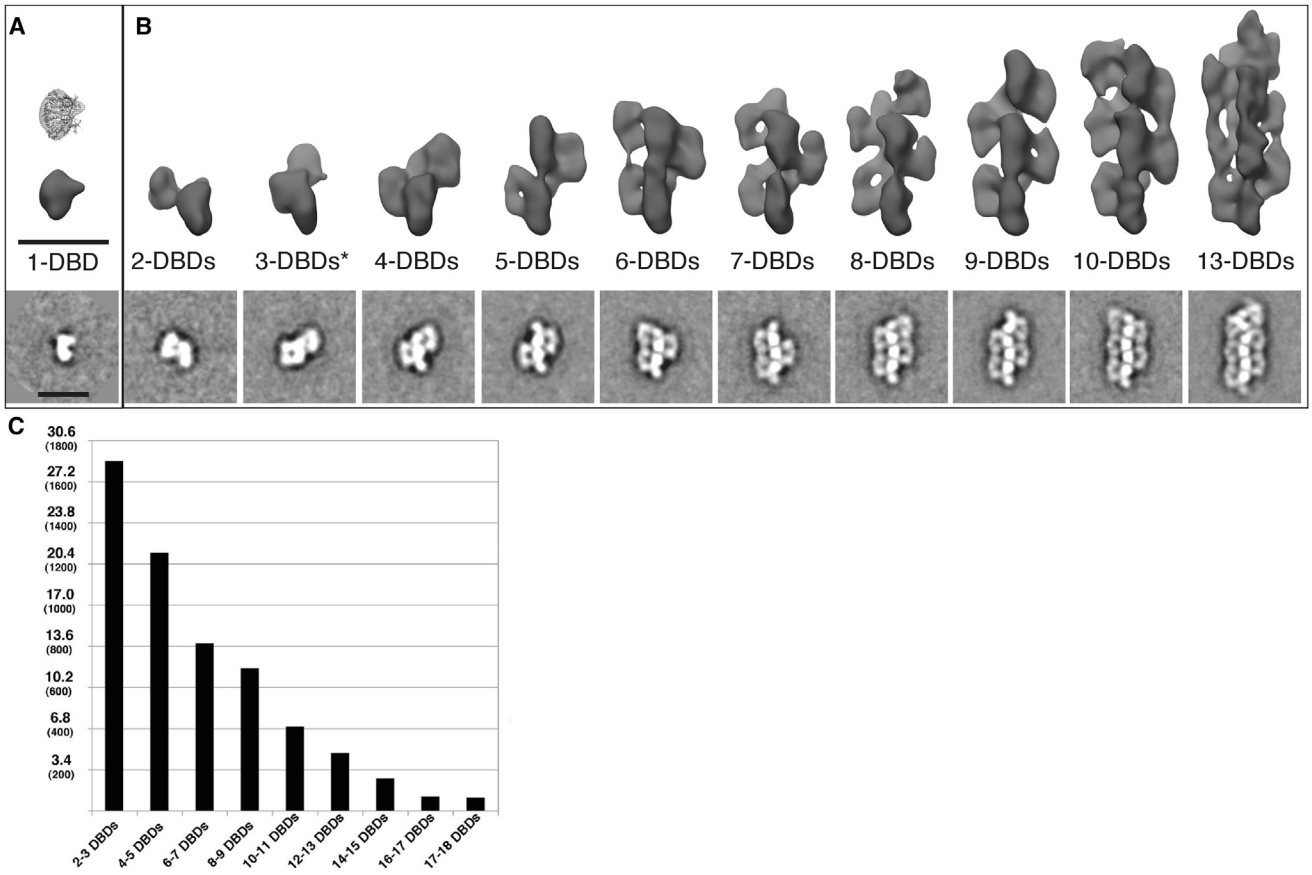

Figure 1. SgrAI Forms Run-On Oligomers in the Presence of Activating DNA

(A and B) 2D class averages and corresponding 3D EM density maps created by the random-conical tilt reconstruction strategy are displayed for (A) a single SgrAI DBD with the corresponding crystal structure (Dunten et al., 2008) displayed above, and subsequently for (B) elongating oligomers. Scale bars represent 150 Å.
*The 3-DBD oligomers adopt an alternative orientation on the EM grid and, their 3D maps are therefore rotated to correspond to the 2D average.
(C) Oligomer size distribution within the negative stain data set; the *x* axis indicates the number of DBDs represented by a single oligomer identified by 2D classification; the *y* axis indicates the percentage of particles within the full data set corresponding to each DBD grouping, and in parentheses, the absolute number of particles.
See also Figure S1 and Table S2.

monomeric subunit undergoes a rotation and slight vertical extension about and away from its central cleavage core in a twisting fashion (Figure 3A; Movie S2). This movement slightly alters the location of C-alpha residues involved in selectivity for the outer two bp of the DNA recognition sequence, R31 and K96, although the atomic consequences of this alteration, particularly with regard to the protein-DNA interface, remain to be determined.

Unlike its closest homologs—Cfr101, NgoMIV, and Bse634I—SgrAI contains a positively charged region in the outer periphery of the enzyme (Figure 3B), while the rest of the protein is highly electrostatically negative (Figure S4). This region corresponds to the site of apparent contact with flanking DNA within the oligomer (Figure 3C). Previous studies have shown that DNA flanks are required for, and play an allosteric role in activation (Bitinaite and Schildkraut, 2002; Daniels et al., 2003; Hingorani-Varma and Bitinaite, 2003; Little et al., 2011; Park et al., 2010b; Wood et al., 2005). Protein-DNA contacts appear in two positions, which both contact along the minor groove of the DNA. Protein loop 56–60 and DNA-flanks 3–5, as well as protein loop 122–140 and DNA-flanks 6–9 constitute two separate interactions evident in the EM density (Figure 3C). Loop 56–60 contains small, uncharged residues that may interact with the backbone, sugar moieties, or DNA bases, while loop 122–140 contains three Arg residues that may interact with the DNA backbone. Both loops are specific to SgrAI and do not exist within its closest type IIF homologs, which do not form oligomers larger than tetramers. Previous crystal structures of DNA-bound SgrAI dimers show flanking DNA extending outward on both sides of the cleavage site (Dunten et al., 2008; Little et al., 2011; Park et al., 2010a). The EM density from the oligomeric form of the protein cannot accommodate a simple straight extension of idealized B-form DNA. Instead, the DNA makes an approximately 30° bend on either side of the cleavage site in order to interact with neighboring DBDs (Figure 3D). This bend is particularly apparent along the minor groove, at and beyond the site of interaction with SgrAI. Due to apparent disorder in the terminal region, we cannot fit any of the DNA between flanking bp 12–16. DNA is known to

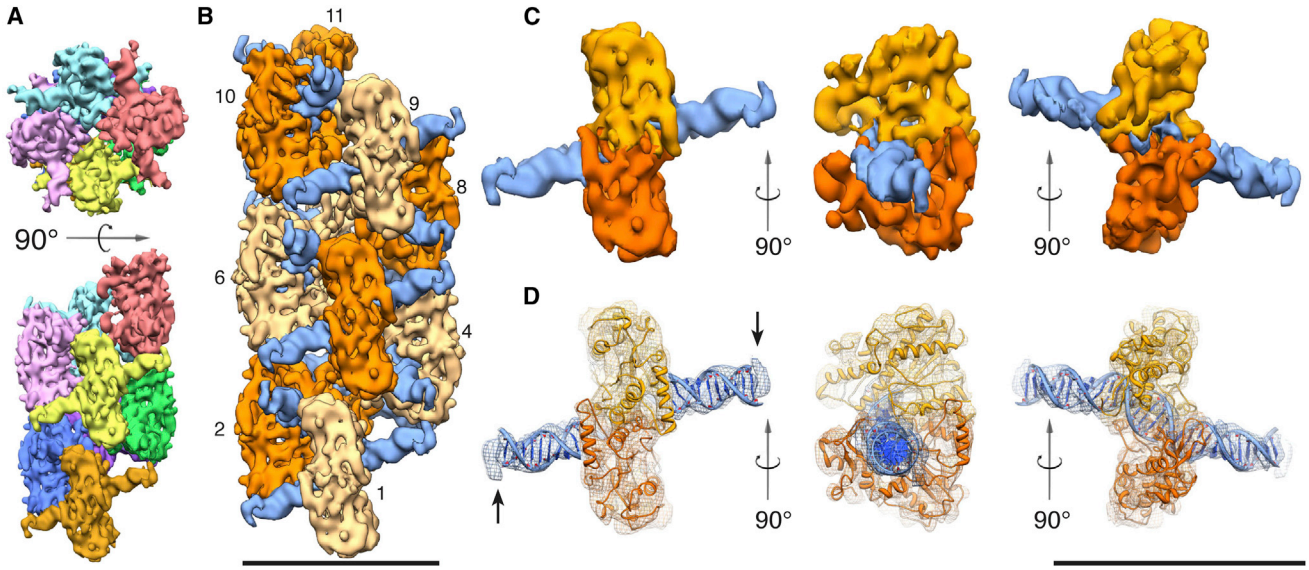

Figure 2. Structure of Activated and Oligomeric SgrAI

(A) Top and side views showing the organization of helical asymmetric units (DBDs) within the SgrAI oligomers. Eight distinct DBDs have been segmented out of the cryo-EM map and are each colored differently.

(B) Helical reconstruction of oligomeric SgrAI at 8.6 Å resolution, segmented into 11 individual DBDs and labeled by helical asymmetric unit. Protein components of units 1,4,6,7,9 and 2,3,5,8,10,11 are shaded light and dark, respectively.

(C) Segmentation and different views of an individual helical asymmetric unit. Each helical asymmetric unit contains two monomeric SgrAI protein subunits (colored light and dark orange), and two copies of precleaved DNA (both colored blue).

(D) Flexibly fit coordinates of SgrAI (Dunten et al., 2008) into the EM density of a segmented helical asymmetric unit. Arrows mark DNA disorder in the terminal regions. Scale bar is 150 Å.

See also Figures S2 and S3 and Movie S1.

exhibit similar local flexibility upon interaction with certain DNA-binding proteins (Peters and Maher, 2010). Thus, the oligomeric form of SgrAI may facilitate stabilization of the DNA bend by slightly repositioning the two protein subunits and providing an allosteric binding site.

SgrAI's N terminus represents another unique region of the protein that is unlike that of its closest homologs (Dunten et al., 2008). It is required for activation because mutation of Pro-27 eliminates oligomerization (Park et al., 2010a). In the oligomeric structure, the N terminus of $DBD_{(n)}$ appears to interact with the N-terminal loop region of $DBD_{(n+1)}$ (amino acids [aa] 21–30; Figure 3E). The EM density does not directly accommodate the type of domain-swapping previously observed (Park et al., 2010a), but there is the possibility that alternative orientations may exist in the oligomeric form. The dissimilarity between SgrAI's N termini and those of its closest homologs, their requirement for oligomerization, and their proximity to each other within the oligomeric structure, support the conclusion that SgrAI's N-terminal interactions facilitate the regulation of its enzymatic activity.

These data show that the oligomeric conformation of SgrAI differs from its dimeric low activity form. The presence of neighboring DBDs and the conformational rearrangement within each individual DBD enable the formation of protein-DNA interactions between its loops and flanking DNA from the nearest neighbors, as well as protein-protein interactions within its N termini. The rearrangement as a whole may have considerable consequences for the positioning of critical residues responsible for enzymatic activity.

SgrAI Activation Requires a Minimum Number of DNA Flanking bp

Previous biochemical studies have recognized the allosteric properties of DNA and indicated that a minimal number of DNA flanking bp must be present for SgrAI activation (Park et al., 2010b; Wood et al., 2005), supporting our structural findings that protein-DNA interactions within the oligomer occur in the vicinity of the DNA minor groove and between flanking bp 3–9. To investigate the precise requirement of flanking DNA length for SgrAI activation, primary-site-containing DNA constructs varying in flanking DNA length and sequence (Table S3) were tested for their ability to stimulate DNA cleavage by SgrAI in single turnover cleavage assays. For both intact and precleaved DNA, greater numbers of flanking bp increased SgrAI activation to a greater extent, with more than eight bp-flanks increasing cleavage up to a rate constant of 22/min (Table 1). All constructs with only five bp-flanks failed to stimulate DNA cleavage despite having low nanomolar affinity for binding (see Park et al., 2010b and Experimental Procedures). Constructs with 6–7 flanking bp provided mixed activation that was somewhat dependent upon the sequence of DNA used (and in some cases the ability of the DNA to remain annealed and/or intact), while all constructs containing 8 bp-flanks effectively stimulated cleavage. These results indicate that (under the reaction conditions and temperature at which cleavage was examined) a minimum of 6 bp-flanks is required for any SgrAI activation. This is consistent with the two allosteric protein-DNA contacts identified within the oligomeric structure that span flanking bp 3–5 and 6–9.

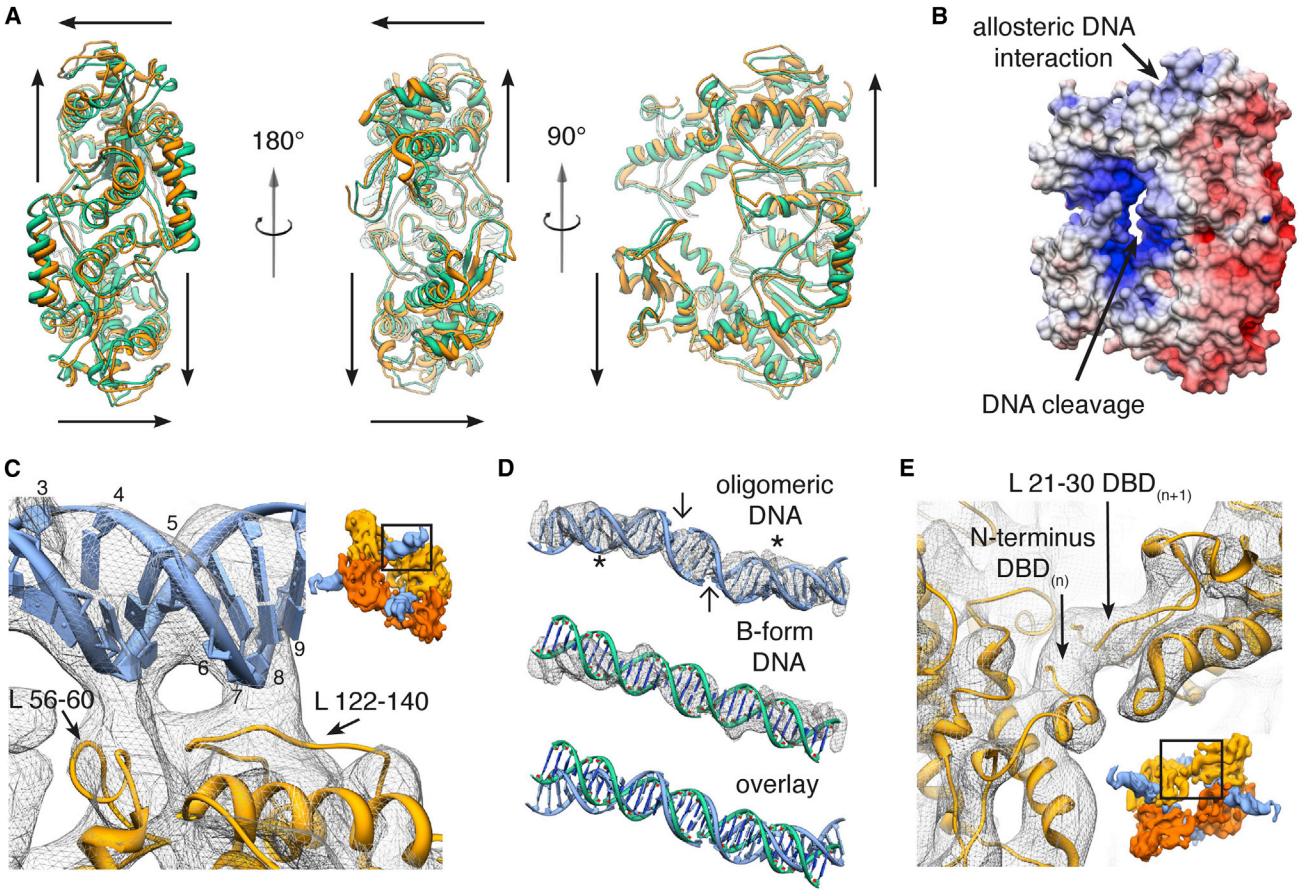

Figure 3. A Conformational Rearrangement Establishes Oligomer-Specific Interactions within Activated SgrAI

(A) Three different views of the crystal structure 3DVO (green; Dunten et al., 2008) are shown overlaid on the flexibly fit coordinates of oligomeric SgrAI (orange). For each DBD, arrows diagram approximate movement from the starting to the ending structure (see also Movie S2).

(B) Surface electrostatic potential of a SgrAI DBD.

(C) Close-up view of protein-DNA interactions within SgrAI's allosteric DNA-binding site, as seen from the outside of the helix (inset). Protein loops 56–60 and 122–140, which are unique to SgrAI, are shown interacting in the vicinity of flanking bp 3–5 and 6–9, respectively (numbered along one DNA strand), and along the minor groove of the DNA.

(D) Comparison of the fit oligomeric PC-DNA with idealized B-form DNA. Oligomeric and B-form DNAs are overlaid on the EM density in mesh. Cleavage sites forming the two precleaved DNAs are marked by arrows. Stars indicate the site of allosteric protein-DNA interaction.

(E) Close-up view of SgrAI's N-terminal interactions, as seen from the inside of the helix (inset). The N terminus of $DBD_{(n)}$ makes apparent interactions with a portion of the N-terminal loop (aa 21–30) of $DBD_{(n+1)}$.

See also Figure S4, Table S1, and Movie S2.

DISCUSSION

In this study, we show that SgrAI will assemble into a regular, repeating structure that is a run-on oligomer formed by the successive helical assembly of individual DBDs. When part of the oligomer, the structure of each of the two subunits comprising the DBD undergoes a large conformational rearrangement compared to the low activity form characterized crystallographically (Dunten et al., 2008; Little et al., 2011; Park et al., 2010a). In this state, SgrAI maintains important interactions within its N termini that are situated in the center of the helical SgrAI oligomer, and with flanking DNA on either side of the cleavage sites. The flanking DNA must contain a minimum of 6 bp to activate the enzyme under the reaction conditions described here; seven, and in particular 8 flanking bp produce increased and more consistent activation. Any additional bp provide little, if any, activation increase. These biochemical results are consistent with our structural findings, which show that the protein-DNA interface occurs in two regions and involves both SgrAI-specific loops and both individual DNA strands of the minor groove (Figures 3B and 3C). Taken together, they suggest that this interface may contain multiple sites of contact along the minor groove, each of which adds a small degree of stability to the interaction as a whole.

SgrAI maintains an enzymatic activity that differs for primary and secondary cleavage sites. Its activity can be drastically altered by the presence of activating DNA, implying intrinsic allostery in its mechanism of action (Bitinaite and Schildkraut, 2002). Structurally, this requires the presence of at least two different conformational states of the enzyme. However, despite the

Table 1. Single Turnover DNA Cleavage Rate Constants of ^{32}P-Labeled DNA 19 in the Presence of Added Unlabeled Intact and/or Precleaved DNA

Added Unlabeled DNA	Type	Length of Flanks (bp)	k_f (min^{-1})[a]	k_s (min^{-1})[a]
1 (PC)[b]	P	16	22 ± 1	N/A
2 (40-1)[b]	I	16	10 ± 1.4 (56 ± 12%)	0.032 ± 0.012 (44 ± 2%)
3	P	10	9.4 ± 1.6	N/A
4	P	8	9 ± 4	N/A
5	P	8	0.54 ± 0.13 (63 ± 17%)	0.08 ± 0.05 (37 ± 17%)
6	I	8	5.4 ± 0.9 (63 ± 1%)	0.04 ± 0.01 (37 ± 1%)
7	P	7	9 ± 1	N/A
8	P	7	2.17 ± 0.17 (80 ± 4%)	0.08 ± 0.04 (20 ± 4%)
8 top	P	7	N/A	0.19 ± 0.02
8 bot	P	7	N/A	0.15 ± 0.03
9	I	7	1.1 ± 0.4	N/A
10	I	7	1.4 ± 0.6 (24 ± 39%)	0.04 ± 0.04 (76 ± 39%)
11	I	7	0.8 ± 0.3 (44 ± 30%)	0.02 ± 0.01 (56 ± 30%)
12	I	7	N/A	0.05 ± 0.03 (100 ± 0%)
13	I	6	N/A	0.13 ± 0.05
14	I	6	1.0 ± 0.6 (79 ± 5%)	0.02 ± 0.002 (21 ± 5%)
15	I	6	N/A	0.14 ± 0.02
16	P	6	N/A	0.13 ± 0.05
17	P	6	N/A	0.15 ± 0.04
18	I	5	N/A	0.09 ± 0.01
19 (18-1)[b]	I	5	N/A	0.16 ± 0.01
20	P	5	N/A	0.20 ± 0.05

"Type" refers to either pre-cleaved DNA (P) or intact DNA (I). "Length of flanking bp" refers to the number of DNA bp outside of the octanucleotide recognition sequence. Values for k_f and k_s refer to rate constants for SgrAI mediated cleavage of 1 nM ^{32}P-labeled DNA 19, derived from fitting the single turnover data. If the data fit significantly better to two rate constants rather than one, the faster rate constant is assigned to k_f, and the slower to k_s. If only a single rate constant is used in the fit, it is assigned to k_f when significantly higher than the rate constant under nonstimulating conditions, and to k_s when similar to that for nonstimulating conditions. The second rate constant is then assigned an N/A because only one rate constant can describe the data. The values are presented as the average of three measurements ± SD.

See also Table S3 for DNA sequences.

[a]Numbers in parentheses indicate the percentage of DNA cleaved by the fast and the slow process in the case when two are present.

[b]Names in parentheses are those used previously for the same DNA constructs (Park et al., 2010b).

biochemical differences, structures of SgrAI bound to both uncleaved (Dunten et al., 2008) and cleaved (Little et al., 2011) primary site DNA, as well as uncleaved secondary site DNA (Little et al., 2011) show few apparent differences. SgrAI bound to primary site DNA favors oligomer formation with either primary (Figure 4A) or secondary (Figure 4B) site DNA. However, in the presence of only secondary site DNA, oligomers do not form (Figure 4C; Park et al., 2010b). Therefore at least one primary site must bind to a neighboring DBD to activate the enzyme (Park et al., 2010b). Furthermore, oligomerization is temperature-dependent, since an identical DNA construct that cannot activate SgrAI at 37°C is capable of low-level activation at 4°C (compare construct 19 in this study to that in Park et al., 2010b). This finding implies that the limited protein-DNA interactions that occur between loop 56–60 and flanking bp 3–5 (Figure 3C) are enough to weakly stabilize the oligomer. Presumably, the enthalpic contribution to oligomer stabilization changes little with increasing temperature, but the entropic contribution increases, and therefore at the higher temperature the limited protein-DNA interactions may be insufficient to overcome entropy leading to dissociation. Maximal stabilization is achieved only when loop 122–140 can efficiently contact bp 6–9 of flanking DNA. These data suggest that SgrAI's two conformational states must exist in equilibrium, that the low activity state may be inactive, and that the differences in enzymatic activity can be explained by SgrAI's ability to access and maintain its high activity form. The oligomer-specific structural features of the enzyme facilitate this maintenance; without sufficient DNA flanks to interact with SgrAI's loops (Figure 3C), oligomerization will not occur (Table 1), nor will it occur without key N-terminal interactions (Park et al., 2010a). This structural and biochemical data allow us to propose that the conformationally rearranged DBD in the oligomeric form stabilizes, and thus represents, the activated enzyme. In sum, SgrAI can cleave both primary and secondary site DNA in the activated conformation, albeit with different cleavage rates, the activated conformation favors oligomerization, and oligomerization in turn favors the activated conformation. The result is both sequence-specificity expansion and/or accelerated DNA cleavage (Figure 4). Future experiments will address the details of this mechanism, in particular with regard to enzyme turnover, including the balance between DBD association and dissociation from the oligomer and the kinetics of DNA release.

Examples of enzyme regulation via run-on oligomerization are relatively uncommon. Recent screens have begun to identify other enzymes capable of self-association into filaments (An et al., 2008; Ingerson-Mahar et al., 2010; Noree et al., 2010; Werner et al., 2009), suggesting that this is a more common phenomenon that previously appreciated. However, the effect of oligomerization on enzyme activity for these enzymes is not currently known. In contrast, the more well-studied NTPases tubulin (Kueh and Mitchison, 2009), actin (Bindschadler et al., 2004), and members of the RecA family (Chen et al., 2008), form run-on oligomers with altered functional properties. Among these systems, it is typically the size, shape, binding behavior, or mechanical properties of the oligomer that is critical for function. While the enzymatic activity of these proteins may be altered with respect to the monomeric form, their substrate specificities remain unchanged. Importantly, the NTPase activity is typically altered to control oligomerization. The converse is true for SgrAI—its main purpose is the enzymatic function of DNA cleavage, and oligomerization appears to modulate enzymatic activity with regard to sequence-specificity expansion (and therefore

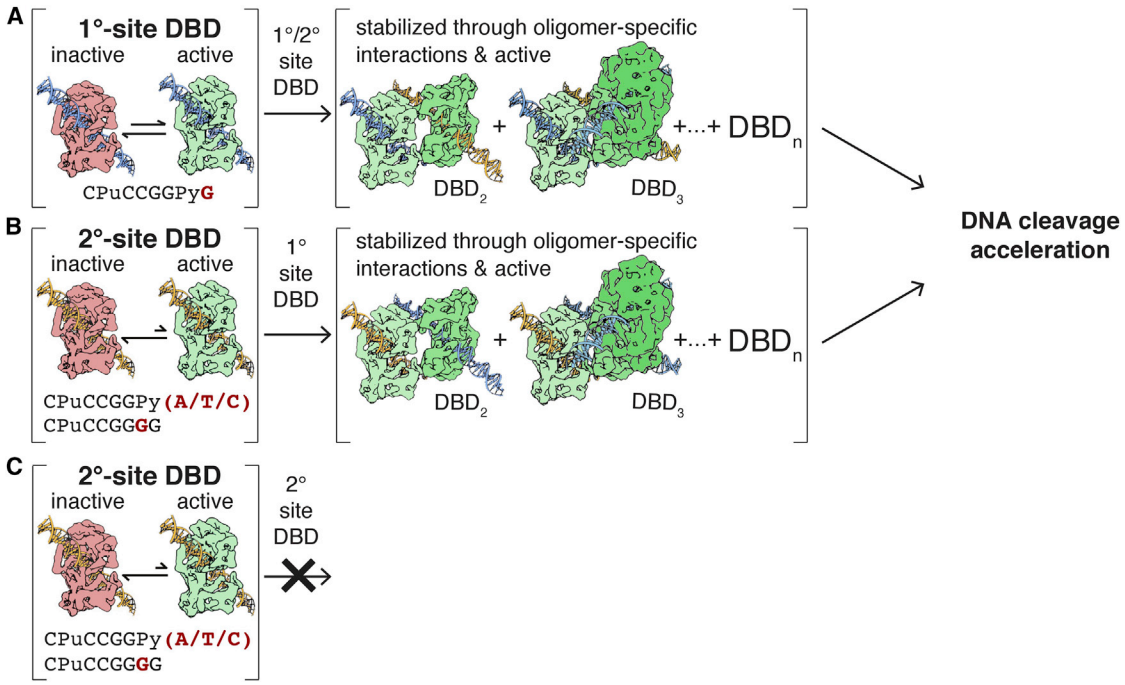

Figure 4. Model of SgrAI DNA-Bound Dimer Activation and Enzymatic Function

SgrAI DBDs contain, at a minimum, two conformational states, which account for an inactive, or minimally active (red), and an active (green) enzymatic state. The two exist in equilibrium, the extent of which is dependent upon whether (A) primary site (blue) or (B and C) secondary site (yellow) DNA is bound. DNA recognition sites are displayed underneath, with the varying nucleotide in red. In the active, dimeric form, both primary and secondary site DNA can undergo cleavage at a slow rate that is determined by the frequency of occupation of the active state. (A) Primary site DBDs can initiate oligomerization, and they can do so with any DBD and regardless of the bound DNA sequence. (B) Secondary site DBDs can join an oligomer containing primary site DBDs. Oligomerization in turn stabilizes the activated conformation and facilitates attachment of additional DBDs, enabling DNA cleavage acceleration (A and B) and/or sequence-specificity expansion (B). To differentiate the distinct subunits, active and stabilized DBDs within the oligomer are shaded differently, although all are presumed to maintain equal activity. (C) Secondary-site DBDs cannot undergo oligomerization by themselves, and higher order species are not observed, although it is possible that transient oligomerzation occurs, but is undetectable under the experimental reaction conditions. The Discussion section provides further mechanistic details.

alteration of substrate specificity) and cleavage rate acceleration. The mechanism by which enzymatic activity is modulated by run-on oligomerization has to our knowledge only been proposed for two other systems—acetyl-CoA carboxylase (ACC) described almost half a century ago (Vagelos et al., 1963), and the unfolded response protein, Ire1 (Korennykh et al., 2009). In the case of ACC, only very modest activation occurs with oligomerizaton (Boone et al., 2000; Brownsey et al., 2006). In the case of Ire1, an RNase activity is thought to switch on as a result of forming run-on oligomers. Neither mechanism involves the alteration of substrate specificity. Therefore, SgrAI's mechanism of activation and alteration of substrate specificity through run-on oligomerization seems to be exceptionally unusual within the enzymatic world.

REases are by definition nonspecific enzymes in that they will cleave DNA of both phage and host. Therefore, in order to perform a protective role against invaders, they must maintain a mechanism through which they can discriminate self from non-self. One hypothesis for the biological function and evolution of SgrAI's protective behavior is related to the unusually large genome of *Streptomyces griseus*, from which the enzyme originates. REases are postulated to protect their bacterial hosts from invading phage DNA, and are prevented from cleaving their host DNA by the action of a cognate methyltransferase that methylates, and thereby protects, the endonuclease target sequence in the host genome. A delicate balance must occur between the activities of the endonuclease and methyltransferase of any such restriction-modification system, such that methylation is conferred to the host, while cleavage to the invader. The large genome of *S. griseus* results in a greater number of potential cleavage sites, and consequently more opportunities for the endonuclease to cause damaging double-stranded DNA cleavage in the host genome. To protect these sites, the cognate methyltransferase would be under selective pressure to methylate at the larger number of sites. To relieve this pressure, the longer recognition sequence of SgrAI may have evolved to reduce the total number of potential cleavage sites within the host genome. Similarly, the relatively slow basal DNA cleavage rate of SgrAI in comparison to other restriction endonucleases (Sam and Perona, 1999) also reduces the potential for DNA cleavage in the competition between methylation and DNA cleavage by the two restriction-modification enzymes. Inevitably, both of these qualities—the longer recognition sequence and the slow DNA cleavage rate—would be expected to reduce the efficacy of the SgrAI endonuclease in protecting against invading phage DNA. Activation by the spatial proximity of two unmethylated recognition sequences, which is expected to be rare in the host genome but very likely in phage DNA, combined

with sequence-specificity expansion from 3 (primary only) to a total of 17 (primary and secondary) different octanucleotide target sequences, would both function to increase the efficacy of SgrAI in protecting against invading phage DNA. However, such functions, particularly the expansion of sequence specificity to sites not potentially methylated by the cognate methyltransferase, could also elicit damaging DNA cleavage to the host. Oligomer formation may thus occur in order to sequester the activated SgrAI endonucleases on phage DNA, and away from the host, representing a clever defensive strategy in the phage-host competition.

EXPERIMENTAL PROCEDURES

Protein and DNA Preparation

Wild-type SgrAI (EC 3.1.21.4) was prepared as described (Dunten et al., 2008) and estimated at 99% purity by Coomassie stained SDS-PAGE. Purified SgrAI enzyme was dialyzed into storage buffer (20 mM Tris-OAc, [pH 8.0], 50 mM KOAc, 0.1 mM EDTA, 1 mM dithiothreitol [DTT], and 50% glycerol), aliquoted into single use aliquots, flash-frozen in liquid nitrogen, and stored at −80°C.

The oligonucleotides (Table S3) used in this study were purchased from a commercial synthetic source, which utilized either gel purification or purification via C18 reverse-phase high-performance liquid chromatography (Aggarwal, 1990). The concentration of the DNA was measured spectrophotometrically, with an extinction coefficient calculated from standard values for the nucleotides (Fasman, 1975). The self-complementary DNA, or equimolar quantities of complementary DNA, were annealed by heating to 90°C for 10 min at a concentration of 1 mM, followed by slow-cooling to 4°C over 4–5 hr in a thermocycler. The concentration of the DNA was remeasured after annealing and presented in terms of duplex DNA. Because multiple freeze-thawing altered the concentration of double-stranded DNA used in the assays by inducing separation of the two strands, DNA constructs used to test for SgrAI activation were aliquoted into single use amounts that were then flash-frozen in liquid nitrogen and stored at −20°C until needed. DNA was 5′ end-labeled with ^{32}P using T4 polynucleotide kinase and [γ-^{32}P]-ATP, and excess ATP was removed using G-30 spin columns.

Sample Preparation for Electron Microscopy

Specimens were prepared for negative stain by applying 3 μl of sample (3 μM SgrAI, 3 μM DNA 1 [PC]; Table S3) in cleavage buffer (10 mM Tris-HCl [pH 8.0], 150 mM NaCl, 5 mM $Mg(OAc)_2$, and 0.5 mM DTT) or binding buffer (10 mM Tris-HCl [pH 8.0], 150 mM NaCl, 5 mM $Ca(OAc)_2$, and 0.5 mM DTT) to a freshly plasma cleaned, continuous carbon grid. The sample was allowed to absorb to the carbon for 30 to 60 s. Excess sample was blotted from the side of the grid and replaced with 2% uranyl formate solution. Specimens were prepared for cryo-EM by applying 3 μl of sample in binding buffer to a holey carbon C-flat grid (CF-2/2-400) (Protochips, inc.) that had been plasma cleaned (Gatan, Solarus) for 5 s. The sample was allowed to adsorb to the grid for 30 s., then plunge-frozen into liquid ethane using a manual cryo-plunger at 4°C.

Electron Microscopy Data Collection of Negatively Stained SgrAI

For the negative stain RCT data set, data were acquired using a Tecnai F20 Twin transmission electron microscope operating at 120 keV, using a dose of 12 × 10^2 Å and a nominal underfocus range of 1 to 3 μm. Images were automatically collected at a nominal magnification of 62,000×, corresponding to a pixel size at the specimen level of 1.76 Å, at 0° and 50° tilt. Images were recorded using a Gatan 4 × 4 K pixel CCD camera utilizing the Leginon data collection software (Suloway et al., 2005).

Random-Conical Tilt Reconstructions of Separate Populations of SgrAI

Experimental data were processed by the Appion software package (Lander et al., 2009), which interfaces with the Leginon database infrastructure. The contrast transfer function (CTF) for each micrograph was estimated using the ACE2 package, a variation of ACE1 (Mallick et al., 2005). CTF correction of the untilted particles was carried out by ace2image during creation of the particle stack, applying a wiener filter with a constant of 0.1. Initially, a small subset of particles was selected using the Difference of Gaussians particle picker (Voss et al., 2009). This provided a preliminary stack, which was aligned and classified in a reference-free manner using the CL2D algorithm (Sorzano et al., 2010). A template was extracted from the class averages and used to automatically select 35,581 tilted and untilted particles from the micrographs using a template-based particle picker (Roseman, 2004). After tilt-pair alignment of the tilted and untilted particle picks with TiltPicker (Voss et al., 2009), 5,442 particle tilt-pairs remained, which were binned by two and extracted using a boxsize of 112 pixels, corresponding to a pixel size of 3.52 Å at the specimen level. The stack was aligned and classified using ISAC (Yang et al., 2012), while maintaining approximately 100 particles per class. Classes representing each distinct SgrAI multimer were aligned to each other to create upright SgrAI references, and these were subsequently used for a reference-based alignment using SPIDER (Frank et al., 1996), followed by multivariate statistical analysis and hierarchical ascendance classification using IMAGIC (van Heel et al., 1996). This step enabled the use of the random-conical tilt pipeline implemented inside Appion (Voss et al., 2010). Particles belonging to each unique class average were reconstructed using the RCT pipeline, and the final volumes were assessed by visual evaluation and from resolution based on the FSC 0.5 criterion. We retained all unique volumes for which, after aligning the central scaffold of the SgrAI oligomer to all distinct RCT volumes, an addition of an SgrAI dimer was observed in either of the two termini at a threshold level that corresponded to the exact size of the SgrAI oligomer. Volumes were discarded based on two criteria: (i) if the volume resulted in a lower resolution than a comparable conformer *and if* combining their particles did not result in an improvement in resolution; and (ii) if the volume lacked sufficient particle numbers to average out noise contributions. Therefore class averages that were separated at the level of classification but produced density maps with less distinguishable SgrAI dimer additions were grouped into a single reconstruction, but only if the result produced an improvement in resolution. From the 5,442 untilted particles, a total of 2,435 were included in the RCT reconstructions. All parameters for the final volumes are summarized in Table S2. Based on these parameters, the average rise and twist were approximated as 21 Å and −90°, respectively. These were used to initiate the refinement of helical filaments. Alignment of the volumes to their central scaffold was performed manually in Chimera (Pettersen et al., 2004).

Oligomer Size Distribution

An alignment and classification of a 6,505-particle stack was performed with CL2D (Sorzano et al., 2010), using a boxsize of 564 Å to accommodate the largest oligomers, and specifying 256 classes (~25 particles per class) for finer class separation. The number of DBDs accounting for each class average was manually summed. The final distribution histogram is shown in Figure 1C, where the data were merged into two-dimer bins.

Cryo-Electron Microscopy Data Collection, Raw-Frame Alignment, and Dose-Fractionation of SgrAI

Data were acquired using the Leginon software (Suloway et al., 2005) installed on a Tecnai F20 Twin transmission electron microscope operating at 200 kV, with a dose of 40 × 10^2 Å and a nominal underfocus ranging from 1 to 4 μm. The dose was fractionated over 20 raw frames collected on the Direct Electron DE-12 direct detection device, with each frame receiving a dose of 2 × 10^2 Å. Six hundred fifty-six "movies" were automatically collected and recorded at a nominal magnification of 29,000×, corresponding to a pixel size of 1.42 Å at the specimen level. The individual frames were aligned using a Spider script that tracks the shifts between individual frames, in a manner similar to that described in Campbell et al., 2012, but without frame averaging. Two raw-frame stacks were created, from which particles were subsequently extracted—the first contained eight aligned frames with a total dose of 16 × 10^2 Å, while the second contained 16 aligned frames, corresponding to a total dose of 32 × 10^2 Å.

Refinement of the SgrAI Helix

The RCT reconstruction of an SgrAI nonamer was used as an initial model for helical refinement of the negative stain data set. Helical refinement was performed using the IHRSR routine implemented in the SPARX package (Behrmann et al., 2012; Hohn et al., 2007). Raw particles used in the refinement

were selected based on the criterion that at least eight SgrAI dimers are present, as judged by the corresponding class averages to which they belong. This provided 1,645 particles for the refinement, aligned along the oligomerization axis, and the refinement was carried out so that the outer radius of alignment would not exceed the radius of an SgrAI octamer. The helical refinement from the RCT initial model was subsequently used to initiate refinement of the cryo-data. For the cryo-EM data set, 691 filaments were selected from 322 raw-frame aligned cryo-micrographs of SgrAI, whose CTF parameters were determined using CTFFind. These filaments were heterogeneous in overall length. Helical segments were windowed at 23 Å intervals using a box size of 272 Å (192 pixels at a pixel size of 1.42), i.e., slightly larger than the length of a helically asymmetric unit (Behrmann et al., 2012), and corresponding to ~90% overlap (Sachse et al., 2007). This provided 7,674 helical segments. We first conducted 25 iterations of the IHRSR routine (Behrmann et al., 2012) to refine the full cryo-data set and obtain final helical parameters: −86.2° helical twist and 21.6 Å rise. Subsequently, the model from IHRSR was used for refinement in Frealign (Grigorieff, 2007) specifying different dose-fractionated stacks for the refinement (32 × 10^2 Å) and reconstruction (16 × 10^2 Å) routines. The final reconstruction was obtained from 1,918 filament segments (25% of the data), averaged eight times to account for the helical symmetry. To avoid overfitting, we used the resolution-limited method for refinement (Stewart and Grigorieff, 2004). The resolution of the refinement was limited to 15 Å until the last several iterations, at which point individual particles were allowed to refine to 12 Å. Two-fold symmetry perpendicular to the helical axis was applied after the refinement and reconstruction procedure by averaging two identical maps, where one has an equivalent rotation about the XZ plane. Incorporation of two-fold symmetry in the refinement and reconstruction process had minimal effects on the nominal resolution value and did not provide obvious improvements to the map over its application postreconstruction. The progression from the initial to the refined model is displayed in Figure S3.

Flexible Fitting of the SgrAI Core into the Cryo-EM Reconstruction

To determine the conformation of the activated enzyme, an isolated map of the SgrAI DBD was obtained using Segger (Pintilie et al., 2010) through the Chimera interface (Pettersen et al., 2004). A model of SgrAI bound to PC DNA generated using the X-ray crystal structure of SgrAI bound to an 18-bp DNA containing a primary site (Protein Data Bank [PDB] ID: 3DVO) and additional modeled flanking DNA in B form was flexibly fitted using Direx (Schröder et al., 2007), a geometry-based conformational sampling approach under low-resolution restraints. The refinement procedure was run for 500 steps followed by the minimization procedure of 300 steps. The following changes in the parameter set were incorporated: the radius used to compute the gradient for each atom (map_probe_sig) was set to 0.5 Å, the number of elastic restraints (den_no) was set equal to the twice the number of atoms in the system, the strength of the elastic network (den_strength) was increased to 0.4, the residue range for DEN restraints (den_resid_range) was set to 30, and the γ parameter (den_gamma) was set to 0 to avoid any optimization for individual proteins.

Electrostatic Calculations

Electrostatic calculations were performed using the APBS web server (http://www.poissonboltzmann.org; Baker et al., 2001) using default parameters.

Single Turnover DNA Cleavage Assays

Single turnover DNA cleavage measurements were performed as described previously (Park et al., 2010b) using rapid chemical quench techniques and 5′ end ^{32}P-labeled oligonucleotide substrates (typically 1.0 nM), under conditions of excess enzyme (1.0 μM), with and without the additional unlabeled DNA. All reactions were performed at 37°C in 20 mM Tris-OAc (pH 8.0), 50 mM KOAc, 10 mM $Mg(OAc)_2$, and 1 mM DTT. Reactions were initiated by mixing 50 μl containing the DNA (1.0 nM ^{32}P-labeled and 0.5–1.0 μM unlabeled) in reaction buffer with 50 μl of enzyme (1.0 μM SgrAI) also in reaction buffer. Both solutions were preheated for 5 min at 37°C. At various times after mixing, 5 μl aliquots were withdrawn and quenched by addition to 5 μl of quench (80% formamide, 50 mM EDTA). Samples were stored at −20°C until they could be electrophoresed on 20% denaturing polyacrylamide (19:1 acrylamide:bisacrylamide, 4 M urea, 89 mM Tris, 89 mM boric acid, and 2 mM EDTA) gels. Autoradiography of gels was performed without drying and a phosphor image plate exposed at 4°C for 12–17 hr. Densitometry of phosphor image plates was performed with a Typhoon Scanner (GE Healthcare Life Sciences), and integration using ImageQuant (GE Healthcare Life Sciences) or ImageJ (Abràmoff and Magalhães, 2004). The percent of product formed as a function of time was determined by integrating the density of both cleaved and uncleaved DNA bands, and normalizing to the total amount cleaved. The single turnover DNA cleavage rate constant was determined from the data using a single exponential function:

$$\%\text{product} = C_1 + C_2 * \left(1 - e^{-kt}\right),$$

where C_1 is a constant fitting the baseline, C_2 is the total percent of DNA predicted to be cleaved by SgrAI, k is the rate constant, and t is the length of incubation in minutes. The data from some reactions fit poorly to a single exponential function. These were found to fit well to the sum of two exponential functions:

$$\%\text{product} = C_1 + C_2 * \left(1 - e^{-k1t}\right) + C_3 * \left(1 - e^{-k2t}\right),$$

where C_1 is a constant fitting the baseline, C_2 is the total percent of DNA predicted to be cleaved by SgrAI with rate constant k_1, C_3 is the total percent of DNA predicted to be cleaved by SgrAI with rate constant k_2, and t is the length of incubation in minutes. The rate constants are presented in Table 1 as k_f and k_s, where k_f is the greater (faster) of the two rate constants k_1 and k_2, and k_s is the lower (slower). For reactions fit by a single rate constant, the rate constant is listed as k_f or k_s in Table 1 depending on whether it was significantly greater than or similar to the unactivated rate constant (0.094 ± 0.015 min^{-1}; Park et al., 2010b), respectively. Measurements were performed at least three independent times and presented as the average ± SD (Table 1).

DNA Binding Assays

The gel shift assay (Carey, 1991) was used to measure the binding affinity of SgrAI to DNA 18 (Table 1; Table S3) in the manner described previously (Park et al., 2010b). The equilibrium dissociation constant (K_D) for DNA 18 was determined to be 0.6 ± 0.1 nM, nearly identical to the 0.6 ± 0.2 nM for DNA 19 determined previously (Park et al., 2010b; Table 1; Table S3).

ACCESSION NUMBERS

The EMDB accession code for the cryo-EM reconstruction of oligomeric SgrAI and the segmented DBD subunit reported in this paper is EMD-2441. The PDB accession code for the flexibly fit C-alpha coordinates reported in this paper is 4C3G.

SUPPLEMENTAL INFORMATION

Supplemental Information includes four figures, three tables, and two movies and can be found with this article online at http://dx.doi.org/10.1016/j.str.2013.08.012.

ACKNOWLEDGMENTS

We would like to thank New England Biolabs for the kind gift of SgrAI enzyme and Arne Moeller for help with figure graphics. This project was supported by grants from the National Science Foundation (NSF 0744732 to F.T. and N.C.H.) and the National Center for Research Resources (RR017573) and the National Institute of General Medical Sciences (GM103310) from the National Institutes of Health (to B.C. and C.S.P.).

Received: June 7, 2013
Revised: August 8, 2013
Accepted: August 9, 2013
Published: September 19, 2013

REFERENCES

Abràmoff, M.D., and Magalhães, P.J. (2004). Image processing with ImageJ. Biophotonics Int. *11*, 36–42.

Aggarwal, A.K. (1990). Crystallization of DNA binding proteins with oligodeoxynucleotides. Methods *1*, 83–90.

An, S., Kumar, R., Sheets, E.D., and Benkovic, S.J. (2008). Reversible compartmentalization of de novo purine biosynthetic complexes in living cells. Science *320*, 103–106.

Baker, N.A., Sept, D., Joseph, S., Holst, M.J., and McCammon, J.A. (2001). Electrostatics of nanosystems: application to microtubules and the ribosome. Proc. Natl. Acad. Sci. USA *98*, 10037–10041.

Behrmann, E., Tao, G., Stokes, D.L., Egelman, E.H., Raunser, S., and Penczek, P.A. (2012). Real-space processing of helical filaments in SPARX. J. Struct. Biol. *177*, 302–313.

Bilcock, D.T., Daniels, L.E., Bath, A.J., and Halford, S.E. (1999). Reactions of type II restriction endonucleases with 8-base pair recognition sites. J. Biol. Chem. *274*, 36379–36386.

Bindschadler, M., Osborn, E.A., Dewey, C.F., Jr., and McGrath, J.L. (2004). A mechanistic model of the actin cycle. Biophys. J. *86*, 2720–2739.

Bitinaite, J., and Schildkraut, I. (2002). Self-generated DNA termini relax the specificity of SgrAI restriction endonuclease. Proc. Natl. Acad. Sci. USA *99*, 1164–1169.

Boone, A.N., Chan, A., Kulpa, J.E., and Brownsey, R.W. (2000). Bimodal activation of acetyl-CoA carboxylase by glutamate. J. Biol. Chem. *275*, 10819–10825.

Brownsey, R.W., Boone, A.N., Elliott, J.E., Kulpa, J.E., and Lee, W.M. (2006). Regulation of acetyl-CoA carboxylase. Biochem. Soc. Trans. *34*, 223–227.

Campbell, M.G., Cheng, A., Brilot, A.F., Moeller, A., Lyumkis, D., Veesler, D., Pan, J., Harrison, S.C., Potter, C.S., Carragher, B., and Grigorieff, N. (2012). Movies of ice-embedded particles enhance resolution in electron cryo-microscopy. Structure *20*, 1823–1828.

Carey, J. (1991). Gel retardation. Methods Enzymol. *208*, 103–117.

Chen, Z., Yang, H., and Pavletich, N.P. (2008). Mechanism of homologous recombination from the RecA-ssDNA/dsDNA structures. Nature *453*, 489–494.

Daniels, L.E., Wood, K.M., Scott, D.J., and Halford, S.E. (2003). Subunit assembly for DNA cleavage by restriction endonuclease SgrAI. J. Mol. Biol. *327*, 579–591.

Dunten, P.W., Little, E.J., Gregory, M.T., Manohar, V.M., Dalton, M., Hough, D., Bitinaite, J., and Horton, N.C. (2008). The structure of SgrAI bound to DNA; recognition of an 8 base pair target. Nucleic Acids Res. *36*, 5405–5416.

Fasman, G.D. (1975). CRC Handbook of Biochemistry and Molecular Biology. (Boca Raton, FL: CRC Press).

Frank, J., Radermacher, M., Penczek, P., Zhu, J., Li, Y., Ladjadj, M., and Leith, A. (1996). SPIDER and WEB: processing and visualization of images in 3D electron microscopy and related fields. J. Struct. Biol. *116*, 190–199.

Grigorieff, N. (2007). FREALIGN: high-resolution refinement of single particle structures. J. Struct. Biol. *157*, 117–125.

Hingorani-Varma, K., and Bitinaite, J. (2003). Kinetic analysis of the coordinated interaction of SgrAI restriction endonuclease with different DNA targets. J. Biol. Chem. *278*, 40392–40399.

Hohn, M., Tang, G., Goodyear, G., Baldwin, P.R., Huang, Z., Penczek, P.A., Yang, C., Glaeser, R.M., Adams, P.D., and Ludtke, S.J. (2007). SPARX, a new environment for Cryo-EM image processing. J. Struct. Biol. *157*, 47–55.

Ingerson-Mahar, M., Briegel, A., Werner, J.N., Jensen, G.J., and Gitai, Z. (2010). The metabolic enzyme CTP synthase forms cytoskeletal filaments. Nat. Cell Biol. *12*, 739–746.

Korennykh, A.V., Egea, P.F., Korostelev, A.A., Finer-Moore, J., Zhang, C., Shokat, K.M., Stroud, R.M., and Walter, P. (2009). The unfolded protein response signals through high-order assembly of Ire1. Nature *457*, 687–693.

Kueh, H.Y., and Mitchison, T.J. (2009). Structural plasticity in actin and tubulin polymer dynamics. Science *325*, 960–963.

Lander, G.C., Stagg, S.M., Voss, N.R., Cheng, A., Fellmann, D., Pulokas, J., Yoshioka, C., Irving, C., Mulder, A., Lau, P.-W., et al. (2009). Appion: an integrated, database-driven pipeline to facilitate EM image processing. J. Struct. Biol. *166*, 95–102.

Little, E.J., Dunten, P.W., Bitinaite, J., and Horton, N.C. (2011). New clues in the allosteric activation of DNA cleavage by SgrAI: structures of SgrAI bound to cleaved primary-site DNA and uncleaved secondary-site DNA. Acta Crystallogr. D Biol. Crystallogr. *67*, 67–74.

Lyumkis, D., Doamekpor, S.K., Bengtson, M.H., Lee, J.-W., Toro, T.B., Petroski, M.D., Lima, C.D., Potter, C.S., Carragher, B., and Joazeiro, C.A.P. (2013). Single-particle EM reveals extensive conformational variability of the Ltn1 E3 ligase. Proc. Natl. Acad. Sci. USA *110*, 1702–1707.

Ma, X., Shah, S., Zhou, M., Park, C.K., Wysocki, V.H., and Horton, N.C. (2013). Structural analysis of activated SgrAI-DNA oligomers using ion mobility mass spectrometry. Biochemistry *52*, 4373–4381.

Mallick, S.P., Carragher, B., Potter, C.S., and Kriegman, D.J. (2005). ACE: automated CTF estimation. Ultramicroscopy *104*, 8–29.

Noree, C., Sato, B.K., Broyer, R.M., and Wilhelm, J.E. (2010). Identification of novel filament-forming proteins in Saccharomyces cerevisiae and Drosophila melanogaster. J. Cell Biol. *190*, 541–551.

Park, C.K., Joshi, H.K., Agrawal, A., Ghare, M.I., Little, E.J., Dunten, P.W., Bitinaite, J., and Horton, N.C. (2010a). Domain swapping in allosteric modulation of DNA specificity. PLoS Biol. *8*, e1000554.

Park, C.K., Stiteler, A.P., Shah, S., Ghare, M.I., Bitinaite, J., and Horton, N.C. (2010b). Activation of DNA cleavage by oligomerization of DNA-bound SgrAI. Biochemistry *49*, 8818–8830.

Peters, J.P., 3rd, and Maher, L.J. (2010). DNA curvature and flexibility in vitro and in vivo. Q. Rev. Biophys. *43*, 23–63.

Pettersen, E.F., Goddard, T.D., Huang, C.C., Couch, G.S., Greenblatt, D.M., Meng, E.C., and Ferrin, T.E. (2004). UCSF Chimera—a visualization system for exploratory research and analysis. J. Comput. Chem. *25*, 1605–1612.

Pingoud, A., and Jeltsch, A. (1997). Recognition and cleavage of DNA by type-II restriction endonucleases. Eur. J. Biochem. *246*, 1–22.

Pingoud, A., and Jeltsch, A. (2001). Structure and function of type II restriction endonucleases. Nucleic Acids Res. *29*, 3705–3727.

Pingoud, A., Fuxreiter, M., Pingoud, V., and Wende, W. (2005). Type II restriction endonucleases: structure and mechanism. Cell. Mol. Life Sci. *62*, 685–707.

Pintilie, G.D., Zhang, J., Goddard, T.D., Chiu, W., and Gossard, D.C. (2010). Quantitative analysis of cryo-EM density map segmentation by watershed and scale-space filtering, and fitting of structures by alignment to regions. J. Struct. Biol. *170*, 427–438.

Qiang, B.Q., and Schildkraut, I. (1987). NotI and SfiI: restriction endonucleases with octanucleotide recognition sequences. Methods Enzymol. *155*, 15–21.

Radermacher, M., Wagenknecht, T., Verschoor, A., and Frank, J. (1986). A new 3-D reconstruction scheme applied to the 50S ribosomal subunit of E. coli. J. Microsc. *141*, RP1–RP2.

Radermacher, M., Wagenknecht, T., Verschoor, A., and Frank, J. (1987). Three-dimensional reconstruction from a single-exposure, random conical tilt series applied to the 50S ribosomal subunit of Escherichia coli. J. Microsc. *146*, 113–136.

Roberts, R.J., Vincze, T., Posfai, J., and Macelis, D. (2010). REBASE—a database for DNA restriction and modification: enzymes, genes and genomes. Nucleic Acids Res. *38*(Database issue), D234–D236.

Roseman, A.M. (2004). FindEM—a fast, efficient program for automatic selection of particles from electron micrographs. J. Struct. Biol. *145*, 91–99.

Sachse, C., Chen, J.Z., Coureux, P.D., Stroupe, M.E., Fändrich, M., and Grigorieff, N. (2007). High-resolution electron microscopy of helical specimens: a fresh look at tobacco mosaic virus. J. Mol. Biol. *371*, 812–835.

Sam, M.D., and Perona, J.J. (1999). Catalytic roles of divalent metal ions in phosphoryl transfer by EcoRV endonuclease. Biochemistry *38*, 6576–6586.

Schröder, G.F., Brunger, A.T., and Levitt, M. (2007). Combining efficient conformational sampling with a deformable elastic network model facilitates structure refinement at low resolution. Structure *15*, 1630–1641.

Sorzano, C.O., Bilbao-Castro, J.R., Shkolnisky, Y., Alcorlo, M., Melero, R., Caffarena-Fernández, G., Li, M., Xu, G., Marabini, R., and Carazo, J.M.

(2010). A clustering approach to multireference alignment of single-particle projections in electron microscopy. J. Struct. Biol. *171*, 197–206.

Stern, A., and Sorek, R. (2011). The phage-host arms race: shaping the evolution of microbes. Bioessays *33*, 43–51.

Stewart, A., and Grigorieff, N. (2004). Noise bias in the refinement of structures derived from single particles. Ultramicroscopy *102*, 67–84.

Suloway, C., Pulokas, J., Fellmann, D., Cheng, A., Guerra, F., Quispe, J., Stagg, S., Potter, C.S., and Carragher, B. (2005). Automated molecular microscopy: the new Leginon system. J. Struct. Biol. *151*, 41–60.

Tautz, N., Kaluza, K., Frey, B., Jarsch, M., Schmitz, G.G., and Kessler, C. (1990). SgrAI, a novel class-II restriction endonuclease from Streptomyces griseus recognizing the octanucleotide sequence 5′-CR/CCGGYG-3′ [corrected]. Nucleic Acids Res. *18*, 3087.

Vagelos, P.R., Alberts, A.W., and Martin, D.B. (1963). Studies on the mechnism of activation of acetyl coenzyme A carboxylase by citrate. J. Biol. Chem. *238*, 533–540.

van Heel, M., Harauz, G., Orlova, E.V., Schmidt, R., and Schatz, M. (1996). A new generation of the IMAGIC image processing system. J. Struct. Biol. *116*, 17–24.

Voss, N.R., Yoshioka, C.K., Radermacher, M., Potter, C.S., and Carragher, B. (2009). DoG Picker and TiltPicker: software tools to facilitate particle selection in single particle electron microscopy. J. Struct. Biol. *166*, 205–213.

Voss, N.R., Lyumkis, D., Cheng, A., Lau, P.-W., Mulder, A., Lander, G.C., Brignole, E.J., Fellmann, D., Irving, C., Jacovetty, E.L., et al. (2010). A toolbox for ab initio 3-D reconstructions in single-particle electron microscopy. J. Struct. Biol. *169*, 389–398.

Werner, J.N., Chen, E.Y., Guberman, J.M., Zippilli, A.R., Irgon, J.J., and Gitai, Z. (2009). Quantitative genome-scale analysis of protein localization in an asymmetric bacterium. Proc. Natl. Acad. Sci. USA *106*, 7858–7863.

Wood, K.M., Daniels, L.E., and Halford, S.E. (2005). Long-range communications between DNA sites by the dimeric restriction endonuclease SgrAI. J. Mol. Biol. *350*, 240–253.

Yang, Z., Fang, J., Chittuluru, J., Asturias, F.J., and Penczek, P.A. (2012). Iterative stable alignment and clustering of 2D transmission electron microscope images. Structure *20*, 237–247.

